

1 **Prediction of 3D Cardiovascular Hemodynamics before and after Coronary Artery Bypass**

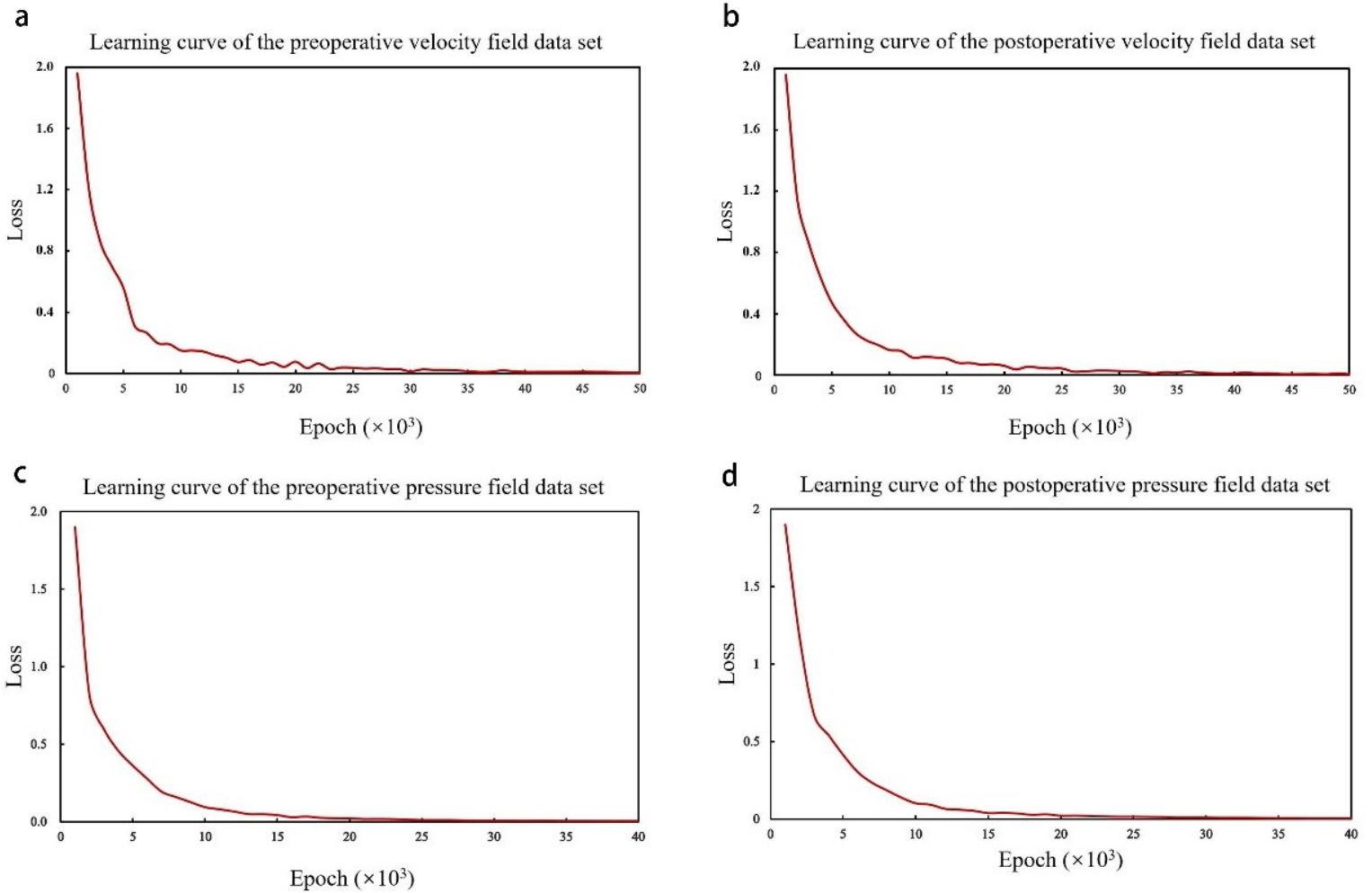
2 **Surgery via Deep Learning**

3 Gaoyang Li et al.

4 **Supplementary Information**

5

6 Supplementary Results



7 **Supplementary Fig. 1** Learning curve. **a-b** are the learning curves of the pre- and post-velocity
8 field datasets. **c-d** are the learning curves of the pre- and post-pressure field datasets. For
9 velocity, the learning curve reaches a minimum when Epoch is about 50K. For pressure, the
10 learning curve reaches a minimum when Epoch is about 40K.

11 **Supplementary Discussion**

12 **Comparison against Previous Deep Learning Approaches**

13 We reviewed studies using deep learning or machine learning for prediction of flow fields or
14 clinical parameters related to CHD treatment (e.g., FFR), as shown in Supplementary Table 1. Itu's
15 machine learning method was only suitable for the calculation of FFR value¹, and its application
16 range was extremely limited. Lee's convolutional neural network could be used for vortex flow
17 prediction in the 2D plane², which might lead to loss of information (such as the flow field
18 component perpendicular to the 2D plane). Guo's deconvolution network is only suitable for 3D
19 regular and simple flow field³. Because the network structure is relatively simple, the above studies
20 all need a large number of data samples to support in order to achieve high prediction accuracy.
21 Although Liang realizes the internal hemodynamic prediction of the ideal thoracic aortic model⁴,
22 the spatial resolution of its samples is still low, which could not accurately characterize the
23 geometric characteristics of complex cardiovascular system. Liang's network only accepts the
24 input data with prefix array-size. This means, patient geometry should be normalized into template
25 (fixed number of meshes). Then, if the geometry cannot fit into that template, Liang's network
26 cannot accept that input. Under the premise of more extensive information, our deep learning
27 method uses limited data to achieve prediction accuracy similar to previous studies. However, our
28 prediction objects are far more complex. Our network can predict the flow on any kind of geometry
29 owing to using the point cloud format. Even the number of point cloud (nodes) varies, our network
30 can accept that unfixed input. Combined with the universality analysis of the network, our deep
31 learning method has many advantages.

32

33 Supplementary Table 1 Comparison analysis of our deep learning method against previous
 34 studies

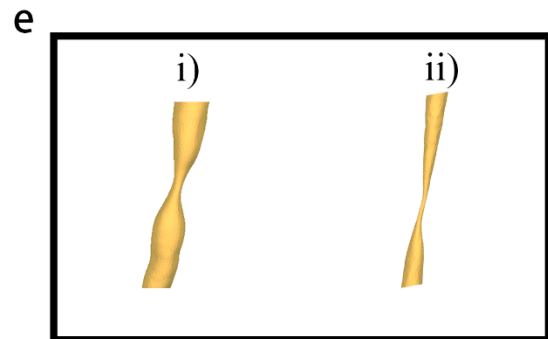
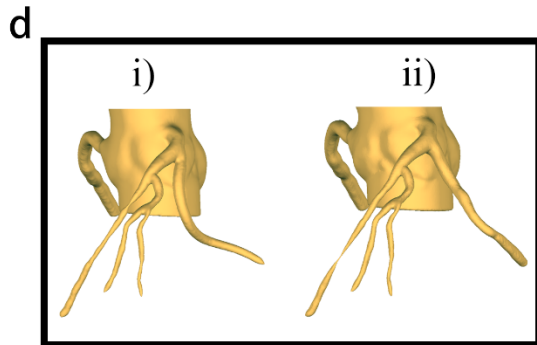
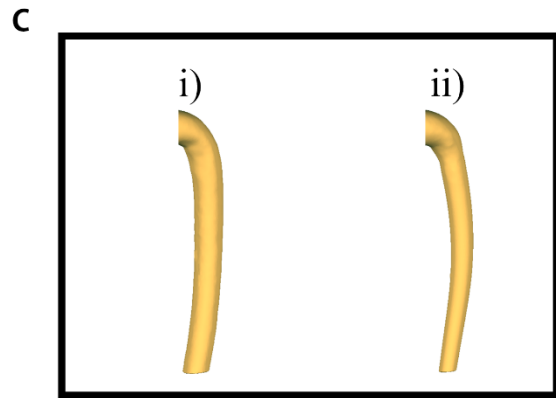
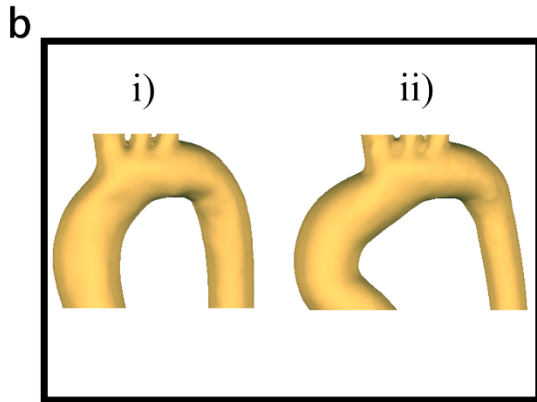
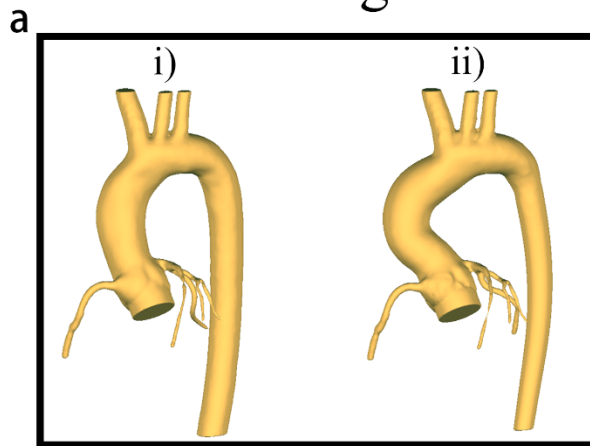
Network or method	Prediction output	Data set size	Input data format	Error function or accuracy
Our Deep Learning Method	3D Patient Personalized Cardiovascular Hemodynamics	1100	High resolution flexible point cloud	NMAE<6.5%, MRE<10%
Itu's Machine Learning Approach ¹	FFR Value	12,000	Geometric parameters	Accuracy= 99.7%
Lee's Adversarial and Convolutional Neural Networks ²	2D Vortex Flow	500000	Grid cells with fixed number	32.8%<Error<1%
Guo's Deconvolution Network ³	3D Regular and Simple Flow	400000	Low resolution pixels with fixed number	MRE<3%
Liang's DNNs ⁴	3D Ideal Thoracic Aorta Hemodynamics	729	Low resolution meshes with fixed number	NMAE<6.5%

35

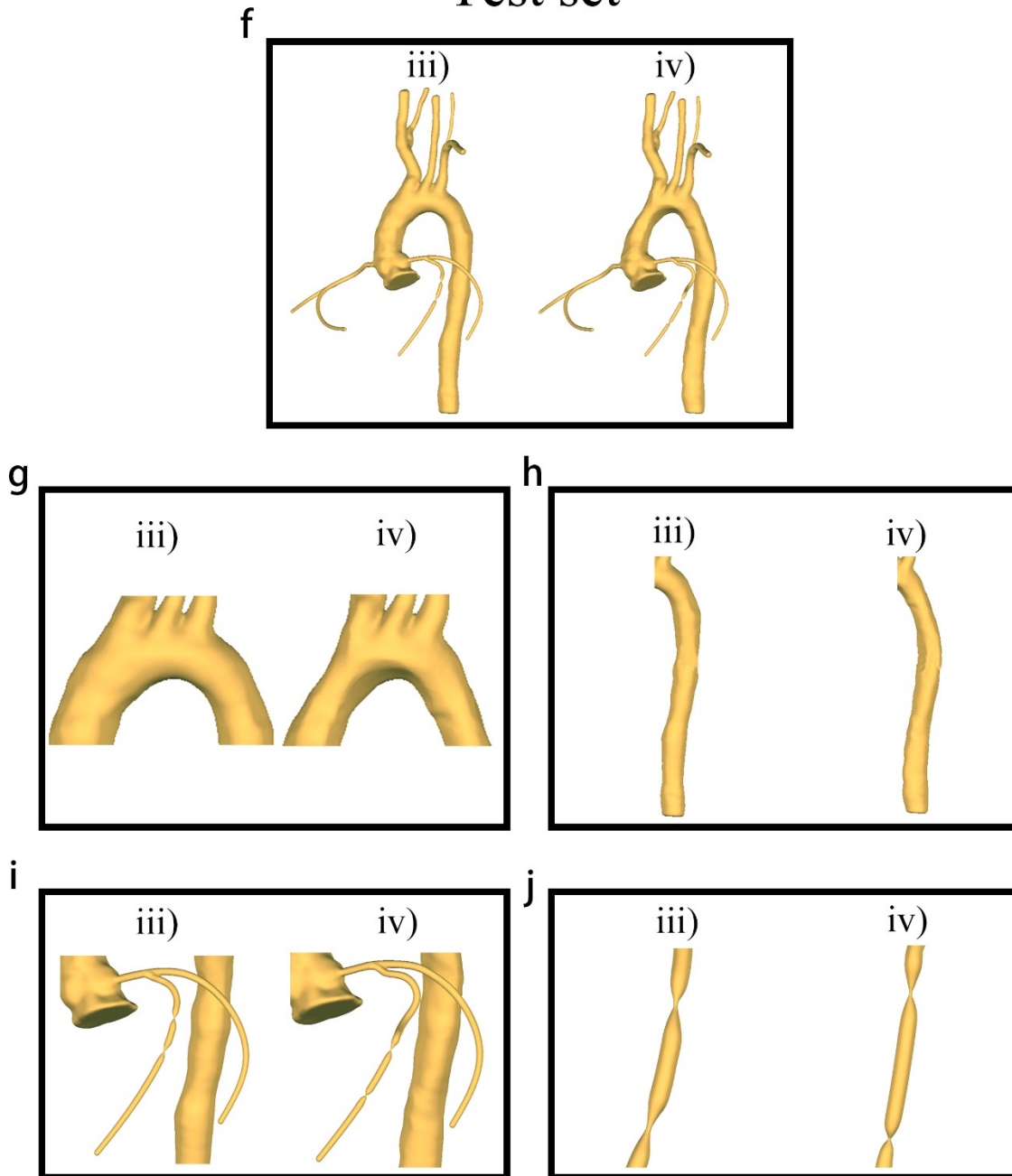
36 **Supplementary Method**
 37 **Model geometric parameters modification**

38 In order to visually show the difference between the models in the training set and the test set, and
 39 to clearly show the modification of the model's geometric structure, we selected a model from the
 40 training set and the test set, and showed the modification results of its geometric structure, as
 41 shown in Supplementary Fig. 2.

Training set



Test set



43

44 **Supplementary Fig. 2** Examples of models in the training and test sets. Examples of models in

45 the training and test sets. i) and iii) is the original model. ii) and iv) is the corresponding modified

46 model. **a** and **f**: overall model; **b** and **g**: ascending aorta and aortic arch angulation; **c** and **h**:

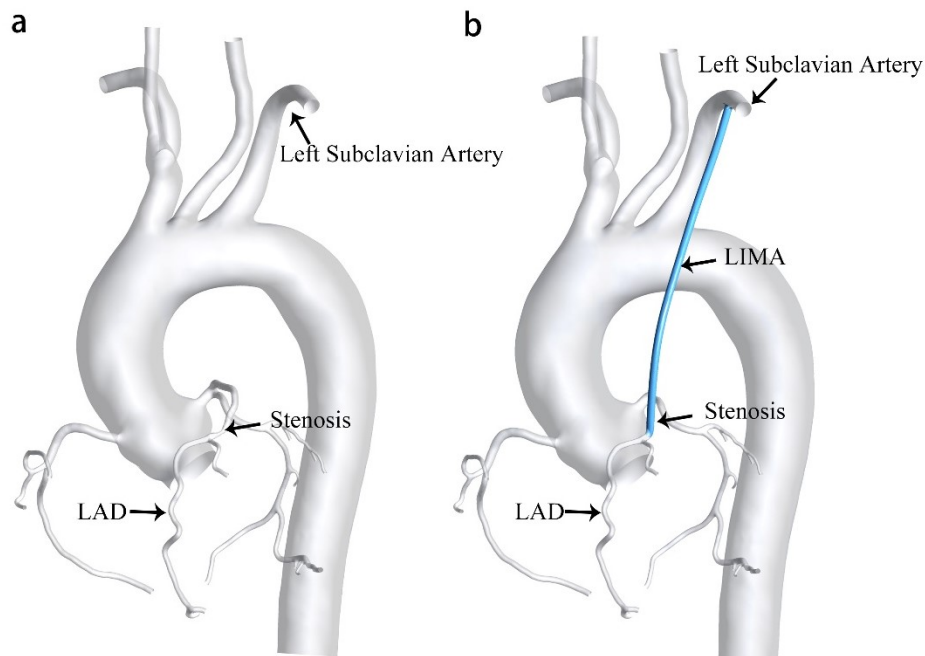
47 descending aorta; **d** and **i**: coronary artery details (LAD and LCX); **e** and **j**: stenosis. All model
48 modifications follow the provisions of Table 3 in the main text.

49 **Simulated operation of CABG and CFD simulation**

50 Among these patient-specific models, except for a few patients who had undergone CABG surgery,
51 the vast majority of patient data had not undergone CABG surgery. Therefore, virtual CABG
52 bypass surgery was performed on these models. According to the recommendations of existing
53 patients and doctors, we chose the left internal mammary artery (LIMA) as the bypass graft. The
54 diameter of the blood vessel was 2 mm following the advice of the doctors. In Supplementary Fig.
55 3, we chose one of the models as an example to show before and after CABG surgery. The
56 operation of virtual surgery was done using the commercially available software Mimics
57 (Materialize NV, BE). Before generating the computational models, the reconstructed 3D models
58 needed to be preprocessed, including surface smoothing and inlet/outlets processing by using the
59 commercially available software Geomagic Wrap (3D system, US). After model preprocessing,
60 tetrahedron-dominant mesh computational models were generated, with maximal sizes of 1.6 mm
61 for the element, for each patient model before and after the CABG procedure using ANSYS-
62 Meshing (ANSYS, Canonsburg, USA). To better capture the flow behaviors, close to the vascular
63 wall, five prismatic boundary layers were generated with a growing ratio of the prism thickness at
64 1.2 mm⁵⁻⁸.

65 The vascular wall was assumed to be rigid and a non-slip condition was assigned at all boundaries.
66 We assumed the blood to be an incompressible Newtonian fluid, with density and viscosity of
67 1050 kg/m³ and 0.0035 Pa s, respectively, and performed steady flow simulations using solver
68 ANSYS-CFX (ANSYS, Canonsburg, USA). Since the FFR calculation needed to be in the state
69 of maximum congestion, a peak wave velocity of 1.125 m/s was imposed as the boundary
70 condition at the inlet⁹. And for the outlets, a fixed static reference zero pressure was applied. The

71 convergence criteria for simulations were chosen as 10^{-4} (Root Mean Square) for the normalized
72 continuity, pressure, and velocity residuals. Upon convergence of each simulation, we extracted
73 four groups of results including preoperative velocity fields and pressure distributions and
74 postoperative velocity fields and pressure distributions and saved them as a CSV file, for further
75 processing and construction of the dataset to be used in deep learning.
76



77

78 **Supplementary Fig. 3** Simulated operation of CABG.

79 **Mesh Independence Test**

80 In this study, the number of nodes ranged from 2.83 to 3.01 million in total across different cases.

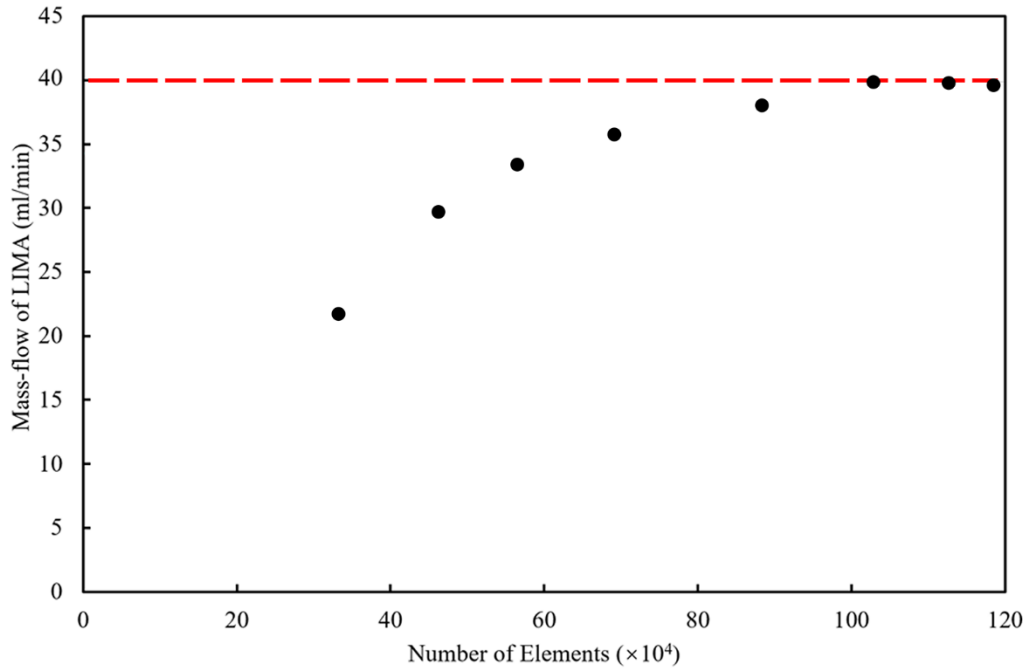
81 In order to reduce errors and make the simulation results stable and reliable, a mesh independence

82 test of computational grids was performed. As shown in Supplementary Fig. 4, the relationship

83 between the mass-flow of LIMA and the number of grids. When the number of meshes exceeds

84 one million, the calculation results can be considered to be stable. Therefore, it is confirmed that

85 the number of grids set in this study was appropriate.



86

87 **Supplementary Fig. 4** Mesh independence test. It confirms that the mesh setting of this study is

88 suitable.

89 **Supplementary References**

- 90 1. Itu, L. *et al.* A machine-learning approach for computation of fractional flow reserve from coronary
 91 computed tomography. *J. Appl. Physiol.* **121**, 42–52 (2016).
- 92 2. Lee, S. & You, D. Prediction of laminar vortex shedding over a cylinder using deep learning. *arXiv*
 93 *Prepr. arXiv1712.07854* (2017).
- 94 3. Guo, X., Li, W. & Iorio, F. Convolutional neural networks for steady flow approximation. in
 95 *Proceedings of the 22nd ACM SIGKDD international conference on knowledge discovery and data*
 96 *mining* 481–490 (2016).
- 97 4. Liang, L., Mao, W. & Sun, W. A feasibility study of deep learning for predicting hemodynamics of
 98 human thoracic aorta. *J. Biomech.* **99**, 109544 (2020).
- 99 5. Taylor, C. A., Hughes, T. J. R. & Zarins, C. K. Finite element modeling of blood flow in arteries.
 100 *Comput. Methods Appl. Mech. Eng.* **158**, 155–196 (1998).
- 101 6. Longest, P. [Worth & Kleinstreuer, C. Comparison of blood particle deposition models for non-
 102 parallel flow domains. *J. Biomech.* **36**, 421–430 (2003).
- 103 7. Chiou, M. C. Particle deposition from natural convection boundary layer flow onto an isothermal
 104 vertical cylinder. *Acta Mech.* **129**, 163–176 (1998).
- 105 8. Dyedov, V. *et al.* Variational Generation of Prismatic Boundary-Layer Meshes for Biomedical
 106 Computing. *Int. J. Numer. Methods Eng.* **79**, 907–945 (2009).

- 107 9. Febina, J., Sikkandar, M. Y. & Sudharsan, N. M. Wall Shear Stress Estimation of Thoracic Aortic
108 Aneurysm Using Computational Fluid Dynamics. *Comput. Math. Methods Med.*
109 <https://doi.org/10.1155/2018/7126532> (2018)